Velocity saturation in few-layer MoS2 transistor

Gianluca Fiori, Bartholomäus N. Szafranek, Giuseppe Iannaccone, and Daniel Neumaier

Citation: Appl. Phys. Lett. **103**, 233509 (2013); doi: 10.1063/1.4840175
View online: http://dx.doi.org/10.1063/1.4840175
View Table of Contents: http://apl.aip.org/resource/1/APPLAB/v103/i23
Published by the AIP Publishing LLC.

Velocity saturation in few-layer MoS_2 transistor

Gianluca Fiori,[1] Bartholomäus N. Szafranek,[2] Giuseppe Iannaccone,[1] and Daniel Neumaier[2]
[1]*Dipartimento di Ingegneria dell'Informazione, Università di Pisa, Via G. Caruso 16, 56122 Pisa, Italy*
[2]*Advanced Microelectronic Center Aachen (AMICA), AMO GmbH, Otto-Blumenthal-Strasse 25, 52074 Aachen, Germany*

(Received 26 August 2013; accepted 19 November 2013; published online 4 December 2013)

In this work, we perform an experimental investigation of the saturation velocity in MoS_2 transistors. We use a simple analytical formula to reproduce experimental results and to extract the saturation velocity and the critical electric field. Scattering with optical phonons or with remote phonons may represent the main transport-limiting mechanism, leading to saturation velocity comparable to silicon, but much smaller than that obtained in suspended graphene and some III–V semiconductors. © *2013 AIP Publishing LLC*. [http://dx.doi.org/10.1063/1.4840175]

Graphene research has shed light on the world of two-dimensional materials, which have recently attracted the interest of the research community, because of their potential to enable and sustain device scaling down to the single-digit nanometer region.

MoS_2 is one of these candidates. As a tangible advantage with respect to graphene, MoS_2 has a band-gap ranging from 1.3 eV to 1.8 eV, depending on the number of atomic layers,[1,2] but on the other hand it has a smaller mobility μ (in single-layer structure of the order of tens of cm^2/Vs (Ref. 3)).

Transistors exploiting MoS_2 as a channel material have been first experimentally demonstrated in Ref. 4, showing large current modulation, when applying supply voltage scaling suggested by the ITRS.[5] A theoretical investigation of their limitations and performance has been addressed in Refs. 6 and 7, and an integrated circuit has been demonstrated in Ref. 8, where a MoS_2-based NAND-gate and a 5-stage ring oscillator have been fabricated.

However, whether MoS_2 can be a promising channel material is an open question, which can be addressed by investigating the main figures of merit related to charge transport in nanoscale devices.

In nanoscale MOSFETs, for high longitudinal electric field, the carrier velocity depends linearly on the longitudinal electric field induced by the drain-to-source voltage only for small fields and then reaches a saturation velocity v_{sat}. As a consequence, understanding the v_{sat} of new materials is of the utmost importance, in order to predict the drain current achievable in operating conditions.

In this work, we extract v_{sat} in FETs with MoS_2 channel, at different temperatures (300–500 K) from purposely fabricated devices. The extracted values show that velocity saturation in MoS_2 is comparable to what obtained in silicon, but almost an order of magnitude smaller as compared to graphene and some III–V materials.

The fabrication procedure is based on the processes used for graphene field-effect transistors.[9] The fabricated device is a backgated MoS_2 field-effect transistor, with channel length $L = 1\,\mu m$ and channel width $W = 1.2\,\mu m$. The MoS_2 layer consists of three atomic layers. We have used highly p-doped Si wafers covered with a 90 nm layer of thermally grown SiO_2 used as a substrate. Subsequently, the MoS_2 layer has been exfoliated with adhesive tape from a natural crystal and deposited on the substrate. Few-layer MoS_2 flakes have been identified using optical microscopy and contrast determination of the MoS_2 relative to the substrate, with a procedure similar to the one known for graphene flakes.[10] After the identification of a flake, the contact electrodes have been fabricated by photolithography, sputter deposition of 40 nm layer of nickel, and a subsequent lift-off process. As we have not observed a channel length dependence of the field effect mobility for devices with channel length ranging from 1 to 8 μm, we can assume a negligible contribution of the contact resistance to the total resistance of our devices. Finally, 44 nm of Al_2O_3 were grown on top of the device using atomic layer deposition. Fig. 1(a) shows the micrograph of a fabricated MoS_2 FET.

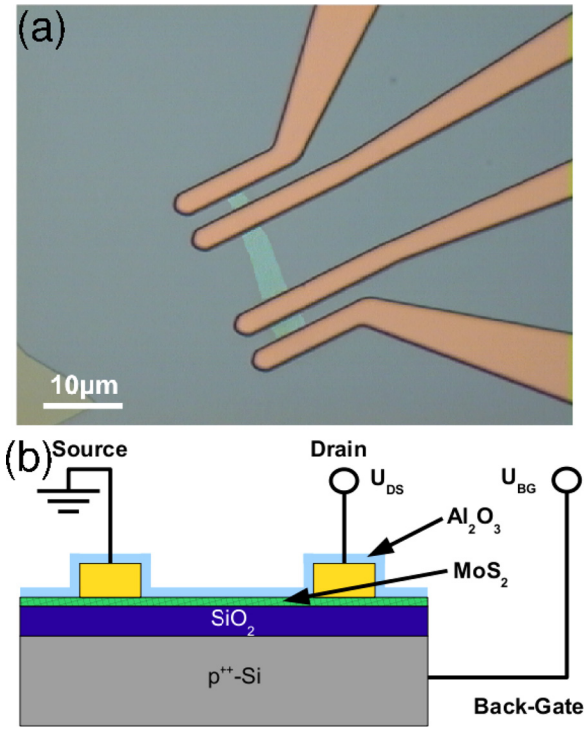

FIG. 1. (a) Micrograph of a MoS_2 FET. The device is covered with an Al_2O_3 layer for passivation. The contrast of the MoS_2 was increased with respect to the surrounding substrate. (b) Schematic longitudinal cross-section of the fabricated device.

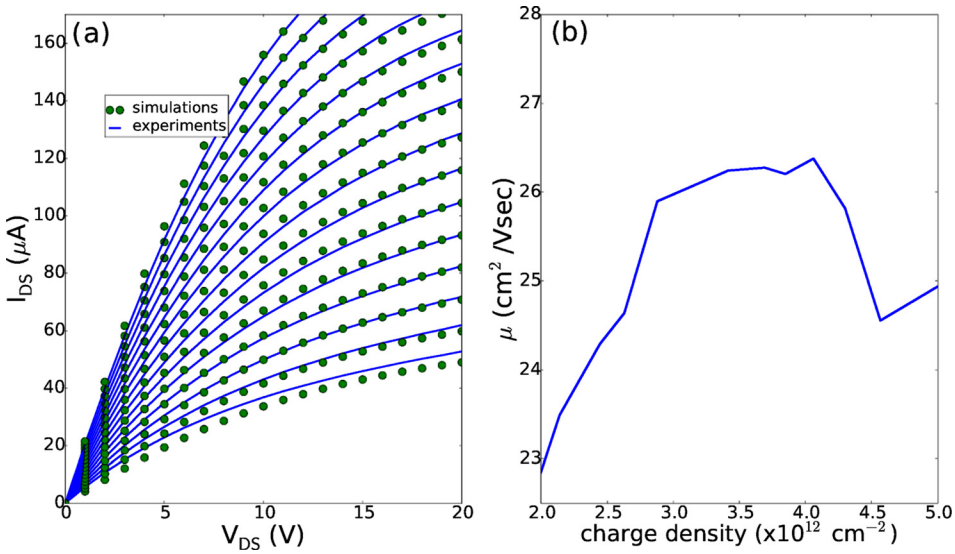

FIG. 2. (a) Measured (solid lines) and computed (dots) output characteristic at room temperature. V_{GS} ranges from 20 to 34 V, with 1 V voltage step. The threshold voltage $V_T = 15$ V. (b) Measured room temperature mobility as a function of V_{GS}.

The device structure is depicted in Fig. 1(b). The samples were measured in a needle probe station at temperature from 294 to 473 K. For the electrical characterization an HP 4156 semiconductor parameter analyzer was used.

We have used the analytical model proposed in Ref. 11 to extract the saturation velocity v_{sat}. In particular, the drain-to-source current (I_{DS}) can be expressed as a function of the channel width and length W and L, respectively, the gate capacitance C_{ox}, the threshold voltage V_T, and the mobility μ as

$$I_{DS} = \frac{W}{L}\mu C_{ox}(V_{GS} - V_T)\frac{V_{DS}}{\left[1 + \left(\frac{V_{DS}\mu}{Lv_{sat}}\right)^{\alpha}\right]^{1/\alpha}}, \qquad (1)$$

where V_{GS} and V_{DS} are the gate-to-source and drain-to-source voltages, respectively, and α has been taken equal to 1.8 — as in Ref. 11 — for all the considered temperatures.

The mobility is extracted directly from experiments in the linear region as

$$\mu = \frac{Lg_m}{WV_{DS}C_{ox}}, \qquad (2)$$

where g_m is the differential transconductance.

Contact resistance has been neglected in Eq. (1), in agreement with experimental observation.

We obtain v_{sat} as a fitting parameter with measured DC characteristics, through a least mean square procedure. In Fig. 2(a), we show the experimental (solid lines) output characteristics at room temperature, for V_{GS} ranging from 20 to 34 V, in steps of 1 V. As can be observed, current in the saturation region depends linearly on V_{GS}, which is a signature of the saturation velocity regime.

In the same picture, we show (dots) the output characteristics given by Eq. (1). The simple analytical model well manages to reproduce the experimental results both in the triode and in the saturation region. In Fig. 2(b), we plot the experimental mobility in the linear region (for $V_{DS} = 0.4$ V) as a function of the charge density in the channel: mobility is almost constant for the considered charge densities and the obtained values are in agreement with mobility in state-of-the-art MoS_2 Field-Effect Transistors.[3]

In Fig. 3, the transfer characteristics both in the logarithmic and linear scale are shown. In Fig. 3(b) we show both experimental transfer characteristics (solid lines) above threshold with the model provided by Eq. (1): results are in good agreement. From the transfer characteristics we can

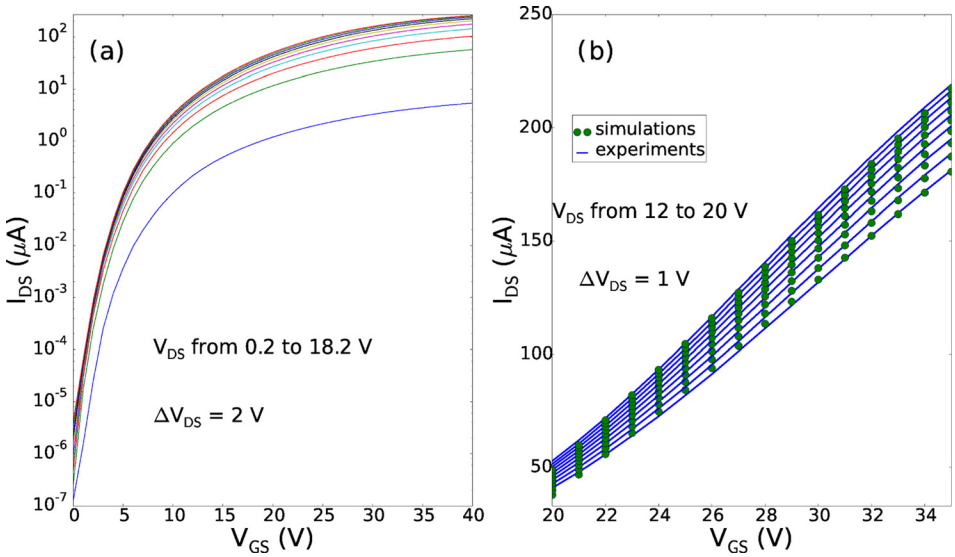

FIG. 3. Experimental transfer characteristics in the (a) semilog and (b) linear scale (solid lines). Dots in (b) represent results from the model in Eq. (1) with fitted values of v_{sat}.

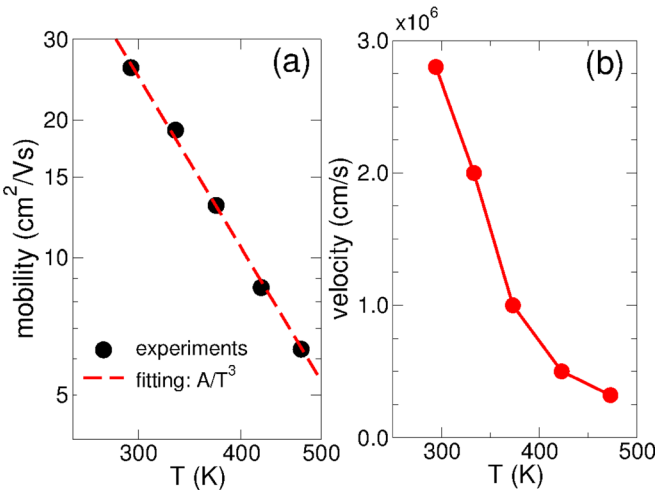

FIG. 4. (a) Mobility as a function of the temperature in the log-log scale. Points refer to the measured mobility while red dashed line to the fitting with the A/T^3 curve. (b) Extracted saturation velocity as a function of temperature.

extract both the sub-threshold swing $SS = 850\,\text{mV/dec}$ and $I_{on}/I_{off} \approx 10^5$.

In Fig. 4(a), mobility is plotted as a function of temperature. Mobility is proportional to $1/T^3$. This dependence can be due either to the dominance of electron-optical phonon coupling (behavior $1/T^{2.6}$ as theoretically demonstrated in Ref. 12) and shown in Ref. 13 or to remote phonons ($1/T^{3.42}$) as experimentally demonstrated in Ref. 14. As expected, this dependence is considerably larger than that foreseen by Density Functional Theory (DFT) calculations in monolayer MoS_2.[2]

In Fig. 4(b), the extracted saturation velocity is shown as a function of temperature: v_{sat} shows a clear dependence on temperature ($v_{sat} \propto 1/T^{3.7}$) while it is independent of V_{GS}, i.e., of the channel carrier density.

Typical known models for velocity saturation, based on the energy balance model or on the electron temperature model,[15] predict a much weaker dependence on temperature, with exponent ranging from −0.5 to −1.5.

One possible reason for the much stronger experimental dependence of v_{sat} on temperature could be the role of thermal activation in transport, which certainly is relevant, also in the relatively high temperature range considered in our study. Indeed, in Table I, we show the extracted threshold voltage and the critical electric field $\xi_{cr} \equiv v_{sat}/\mu$ at different temperatures: V_T exhibits a strong dependence on temperature in the considered temperature range, which has been also observed in Ref. 3 and also in that case explained with thermally activated transport. Complete understanding of v_{sat} dependence on temperature surely deserves further investigation.

In Table II we compare the critical electric field ξ_{cr} and v_{sat} of different materials at room temperature. We can observe that v_{sat} and ξ_{cr} in MoS_2 are similar to those of more common semiconductors, and almost one order of magnitude

TABLE I. Threshold voltage (V_T) and critical electric field $\xi_{cr} = v_{sat}/\mu$.

T (K)	294	333	373	423	473
VT (V)	15	13	9	6	2
ξ_{cr} (MV/cm)	0.115	0.105	0.0769	0.0581	0.0508

TABLE II. Saturation velocity[16,17] and critical electric field ξ_{cr} (Refs. 17 and 18) at room temperature for different materials.

Material	v_{sat} (10^7 cm/s)	ξ_{cr} (V/cm)
MoS_2	0.28	1.15×10^5
Si	1.02	4×10^4
Graphene	5.5	10^5
InSb	5	10^3
GaAs	0.72	0.3×10^4
Ge	0.72	4×10^4
AlAs	0.85	10^5
GaP	0.88	2×10^5
GaN	1.4	…
InGaAs	1.8	…

smaller than those of suspended graphene and III–V materials. Another device with $L = 1\,\mu$m has also been measured, giving a v_{sat} close to the one shown in Table II (i.e., $v_{sat} = 0.27 \times 10^7$ cm/s).

We have extracted the carrier saturation velocity in few-layer MoS_2 MOSFETs both in the linear region and in the saturation region of the DC current-voltage characteristics. The strong temperature dependence of v_{sat} and V_T in the 300–500 K temperature range considered reveals the role played by thermally activated transport. We show that the experimental mobility has a temperature dependence close to T^{-3} compatible with scattering with optical or remote phonons. Complete understanding of the temperature dependence of v_{sat} requires additional investigation. Our results confirm that MoS_2 can be a promising material for electronics: both v_{sat} and ξ_{cr} are comparable to those of common semiconductors, but few-layer MoS_2 has the advantage of being a two-dimensional material, suitable for the realization of few-nm FETs with very good electrostatics. With respect to suspended graphene, both v_{sat} and ξ_{cr} are one order of magnitude lower, but MoS_2 has an adequate energy gap for applications in electronics, even at relatively high temperature.

The work was supported in part by the EC Seventh Framework Program under the STREP project GRADE (Contract 317839) and by the German Science Foundation DFG under the project Ultragraphen.

[1]K. F. Mak, C. Lee, J. Hone, J. Shan, and T. F. Heinz, Phys. Rev. Lett. **105**, 136805 (2010).
[2]K. Kaasbjerg, K. S. Thygesen, and K. W. Jacobsen, Phys. Rev. B **85**, 115317 (2012).
[3]B. Radisavljevic and A. Kis, Nat. Mater. **12**, 815 (2013).
[4]B. Radisavljevic, A. Radenovic, J. Brivio, V. Giacometti, and A. Kis, Nat. Nanotechnol. **6**, 147 (2011).
[5]See http://www.itrs.net for the international technology roadmap for semiconductors. Process integration, devices, and structures, 2011 ed., Chap. 2.
[6]L. Liu, S. B. Kumar, Y. Ouyang, and J. Guo, IEEE Trans. Electron Devices **58**, 3042 (2011).
[7]Y. Yoon, K. Ganapathi, and S. Salahuddin, Nano Lett. **11**, 3768 (2011).
[8]H. Wang, L. Yu, Y.-H. Lee, Y. Shi, A. Hsu, M. L. Chin, L.-J. Li, M. Dubey, J. Kong, and T. Palacios, Nano Lett. **12**, 4674 (2012).
[9]B. N. Szafranek, G. Fiori, D. Schall, D. Neumaier, and H. Kurz, Nano Lett. **12**, 1324 (2012).
[10]P. Blake, E. W. Hill, A. H. C. Neto, K. S. Novoselov, D. Jiang, R. Yang, T. J. Booth, and A. K. Geim, Appl. Phys. Lett. **91**, 063124 (2007).
[11]A. Khakifirooz, O. Nayfeh, and D. Antoniadis, IEEE Trans. Electron Devices **56**, 1674 (2009).
[12]R. Fivaz and E. Mooser, Phys. Rev. **136**, A833 (1964).

[13]A. Betti, G. Fiori, and G. Iannaccone, Appl. Phys. Lett. **98**, 212111 (2011).
[14]J. Chen, C. Jang, S. Xiao, M. Ishigami, and M. S. Fuhrer, Nat. Nanotechnol. **3**, 206 (2008).
[15]M. Lundstrom, *Fundamentals of Carrier Transport*, 2nd ed. (Cambridge University Press, Cambridge, UK, 2000).
[16]R. Quay, C. Moglestue, V. Palankovski, and S. Selberherr, Mater. Sci. Semicond. Process. **3**, 149 (2000).
[17]I. Meric, M. Y. Han, A. F. Young, B. Ozylmaz, P. Kim, and K. L. Shepard, Nat. Nanotechnol. **3**, 654 (2008).
[18]M. Fischetti, IEEE Trans. Electron Devices **38**, 634 (1991).